American Mineralogist, Volume 82, pages 8–15, 1997

Lattice simulation studies of the ferroelastic phase transitions in $(Na,K)AlSi_3O_8$ and $(Sr,Ca)Al_2Si_2O_8$ feldspar solid solutions

MARTIN T. DOVE AND SIMON A.T. REDFERN

Department of Earth Sciences, University of Cambridge, Downing Street, Cambridge CB2 3EQ, U.K.

ABSTRACT

Lattice-energy minimization calculations have been performed on the feldspar systems $(Ca,Sr)Al_2Si_2O_8$ and disordered $(Na,K)AlSi_3O_8$ as functions of composition to simulate the ferroelastic phase transitions $I2/c$–$I\bar{1}$ and $C2/m$–$C\bar{1}$, respectively. In both cases the phase transition occurs as a function of composition and is driven by the vanishing of the quantity $C_{44}C_{66} - C_{46}^2$, without any of the individual elastic constants being strongly dependent on composition and without softening of an optic mode. In both cases, the strains ϵ_4 and ϵ_6 are proportional to each other for small values of strain, but nonlinear coupling becomes dominant when $|\epsilon_4|$ becomes larger than about 0.02. The results are consistent with experimental data and explain the nature of coupling of the displacive transition to Al-Si ordering in Al:Si 2:2 feldspars.

INTRODUCTION

Both the $(Ca,Sr)Al_2Si_2O_8$ "2:2" feldspars and the $(Na,K)AlSi_3O_8$ "1:3" feldspars undergo ferroelastic phase transitions as functions of composition at low temperature. The former display a generally ordered arrangement of Al and Si over the tetrahedral sites, although sometimes with varying degrees of Al-Si order, whereas the ferroelastic phase transition in the alkali feldspars occurs only when the Al and Si are disordered over the tetrahedral sites (equivalent to the monalbite–high-albite transition). The changes in space group are $I2/c$–$I\bar{1}$ and $C2/m$–$C\bar{1}$, respectively. In both cases, if the transition is a proper ferroelastic the stability condition that is broken at the symmetry change is $C_{44}C_{66} - C_{46}^2 > 0$ (Cowley 1976). However, with such ferroelastic phase transitions the question always arises as to whether or not the elastic instability is precipitated by softening of an optic phonon (necessarily at zero wave vector) rather than acoustic softening. Recent theoretical work with the rigid-unit-mode model (Hammonds et al. 1996), applied to the feldspar structure, suggests that there is not an optic instability but that there is considerable softening of the acoustic modes, leading to the possibility that the observed structural phase transitions in these feldspars are due to intrinsic elastic instabilities. It is important to test these predictions, not least because of their implications for the thermodynamic modeling of these phase transitions: If the transition is a proper ferroelastic the spontaneous strain is the order parameter and the excess free energy may be written in terms of this strain explicitly, rather than in terms of some unknown coupled order parameter. It is also of interest to enquire as to how the stability condition $C_{44}C_{66} - C_{46}^2 > 0$ is broken. This may result from softening of either of the individual elastic constants C_{44} or C_{66}, or else the combination $C_{44}C_{66} - C_{46}^2$ might be naturally soft and therefore extremely sensitive to changes in temperature and chemical composition without any of the individual elastic constants softening on their own. Again, this issue has implications for the thermodynamic modeling of the phase transition because different models predict different elastic behavior.

Although there is a large body of information on the crystallographic details of these phase transitions, there is none on the elastic constants. This reflects the experimental difficulty in obtaining good elastic data on well-characterized feldspar crystals as a function of composition or temperature. An alternative to experiment is the use of lattice simulation methods with reliable interatomic potentials. Here we present the results of a study of these phase transitions using static lattice-energy minimization and lattice dynamics calculations using empirical interatomic potentials. We chose to work with a model that simulates complete Al-Si disorder in the alkali feldspars because, in these feldspars, the ordering process results in the same symmetry change as the ferroelastic phase transition. For the alkaline-earth feldspars we calculated the solid solution at varying degrees of Al-Si order and ascertained the relationship between the zone-center ferroelastic instability and the zone-boundary Al-Si ordering process.

The details of the lattice-energy minimization and lattice dynamics calculations have been described in several studies (Price et al. 1987; Catlow 1988; Dove 1989; Winkler et al. 1991; Patel et al. 1991). We used the THBREL and THBPHON programs, which in several ways are particularly suited for the simulation of silicates. The pair interactions between atoms were modeled using the standard Coulomb and Buckingham potentials:

0003–004X/97/0102–0008$05.00

TABLE 1. Numerical values of the parameters used in the model pair potentials

	B (eV)	ρ (Å)	C (eV Å^6)
O···O	22764.0	0.149	27.88
Si···O	1283.9073	0.32052	10.66158
Al···O	1460.3	0.29912	0.0
Na···O	5836.885	0.2387	0.0
K···O	65269.71	0.2130	0.0
Ca···O	6958.3	0.2516	0.0
Sr···O	17314.2	0.24	0.0

Note: Parameters are defined in the text.

TABLE 2. Numerical values of the ionic charges, core-shell potential parameter, and bond-bending potential parameter

	Charge (e)	k (eV rad^{-2})	K (eV Å^6)
O core	0.84819		
O shell	−2.84819		74.92
Si	4	2.09724	
Al	3	2.09724	

Note: Parameters are defined in the text.

$$\varphi(r_{ij}) = \frac{Q_i Q_j}{4\pi\epsilon_0 r_{ij}} - \frac{C}{r_{ij}^6} + B\exp(-r_{ij}/\rho) \quad (1)$$

where the parameters C, B, and ρ depend only on the atom pairs, and the charges Q were assumed to have formal values. The O atoms were treated within the shell model, where the anion is separated into a massless outer shell and an inner massive core, the charge is partitioned between the core and shell, and the core and shell interact by a simple harmonic energy that depends on only the separation d of the positions of the core and shell:

$$\varphi(d) = \tfrac{1}{2}Kd^2. \quad (2)$$

The pair interactions described above are assumed to operate only with the shell component of the O^{2-} anion. The final part of the model involves a term that depends on the angle, θ, that two O atoms subtend at a common bonded Si or Al atom:

$$\varphi(\theta_i,\theta_j) = \tfrac{1}{2}k(\theta_i - \theta_j)^2. \quad (3)$$

This interaction simulates part of the covalency inherent in the SiO_4 and AlO_4 tetrahedra. The parameters used in this model are given in Tables 1 and 2. They comprise a transferable set of parameters obtained by using both empirical and quantum mechanical methods, as described by Price et al. (1987), Catlow (1988), Dove (1989), Winkler et al. (1991), and Patel et al. (1991). The model was thoroughly tested in a wide range of simulations of silicates by these authors and shown to be accurate for a wide range of different silicate structure types. It should be noted that the potentials were not optimized or adjusted for the present study. A measure of the transferability of these potentials is given by a comparison of the results obtained from them for the static lattice minimization of unit cells of the end-member feldspars of interest to us and the observed unit-cell parameters of these structures. From Table 3 we see that the three-body potential model enables the accurate calculation of the structural properties of these feldspars.

Burnham (1990) reviewed some of the earlier computational work on end-member feldspar structures, focusing on the work of Post and Burnham (1987), which used two-body ionic potentials. Since then, further calculations on low albite (Patel et al. 1991) and other ordered microcline and anorthite (Purton and Catlow 1990) have been performed as part of the development of transferable potentials incorporating three-body terms, and the results of empirical fits, modified electron gas methods, and Hartree-Fock calculations. The agreement we obtained between modeled and observed structures (Table 3) is superior to the studies of Post and Burnham (1987) and Patel et al. (1991) and comparable with the accuracy suggested by Purton and Catlow (1990) using the same methods.

Because lattice-energy calculations are effectively classical simulations at absolute zero temperature, we modeled the phase transitions through the dependence of the crystal structure on chemical composition of the alkaline-earth or alkali cations on the M site, changing from Ca^{2+} to Sr^{2+} in one case, and from Na^+ to K^+ in the other. Our procedure used effective potentials for the M sites with an occupancy x of one cation and $(1 - x)$ of the other. These effective potentials were formed using the condition that the first and second differentials of the effective potential should be equal to the weighted mean of the differentials of the pure potentials at the observed atomic separation r_0:

$$\left(\frac{\partial\varphi_{\text{eff}}}{\partial r}\right)_{r=r_0} = x\left(\frac{\partial\varphi_1}{\partial r}\right)_{r=r_0} + (1-x)\left(\frac{\partial\varphi_2}{\partial r}\right)_{r=r_0}$$
$$\left(\frac{\partial^2\varphi_{\text{eff}}}{\partial r^2}\right)_{r=r_0} = x\left(\frac{\partial^2\varphi_1}{\partial r^2}\right)_{r=r_0} + (1-x)\left(\frac{\partial^2\varphi_2}{\partial r^2}\right)_{r=r_0} \quad (4)$$

(Winkler et al. 1991). These conditions lead to equations for the parameters in the functional form of the effective potential, $\varphi_{\text{eff}}(r)$. This procedure is equivalent to making the standard mean-field approximation because it neglects local fluctuations in the ordering. For the present purposes this approximation is not significant. The same method was used to obtain effective potentials for the tetrahedral cations corresponding to various degrees of Al-Si order, with x for the T sites of the alkali feldspars corresponding to 0.25 Al, for example.

The lattice-energy calculations gave two types of results. First, the equilibrium crystal contains information about the distortion of the structure through the monoclinic-to-triclinic spontaneous ferroelastic strains, as given for feldspars by Redfern and Salje (1987). For the monoclinic-to-triclinic phase transitions the important symmetry-breaking strains are

TABLE 3. Comparison of calculated and observed unit-cell parameters for disordered end-member feldspars

	$SrAl_2Si_2O_8$		$CaAl_2Si_2O_8$		$NaAlSi_3O_8$		$KAlSi_3O_8$	
	calc	obs*	calc	obs*	calc	obs**	calc	obs†
a (Å)	8.316	8.395	8.181	8.139	8.180	8.154	8.584	8.539
b (Å)	12.879	12.977	12.874	12.815	12.850	12.869	12.989	13.015
c (Å)	14.037	14.270	14.174	13.890	7.056	7.107	7.134	7.179
α (°)	91.422	90	93.150	93.592	93.205	93.521	90	90
β (°)	115.878	115.440	115.810	117.119	116.985	116.458	115.99	115.99
γ (°)	90.728	90	91.260	90.488	90.310	90.257	90	90

* From McGuinn and Redfern (1994a).
** Results for high albite from Prewitt et al. (1976).
†Results for sanidine from Phillips and Ribbe (1973).

$$\epsilon_4 = \frac{1}{\sin \beta_0^*}\left(\frac{c \cos \alpha}{c_0} + \frac{a \cos \beta_0^* \cos \gamma}{a_0}\right)$$

$$\epsilon_6 = \frac{a \cos \gamma}{a_0} \qquad (5)$$

where the subscript 0 denotes the paraphase value, usually extrapolated from the observed behavior of the high-symmetry phase to the conditions of interest in the stability field of the low-symmetry phase. However, the static lattice calculations allow direct determination of the paraphase cell parameters directly, without recourse to this extrapolation. The second interesting result of the lattice-energy calculations is the elastic constant matrix. The important quantity to be derived from the elastic constant matrix when considering the triclinic-monoclinic behavior of feldspars is the product combination $C_{44}C_{66} - C_{46}^2$.

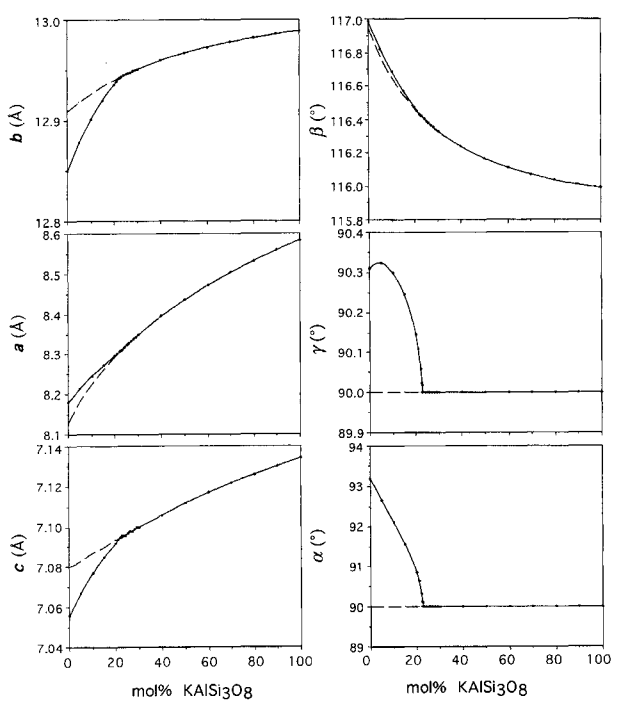

FIGURE 1. Composition dependence of the calculated unit-cell parameters of disordered $(Na,K)AlSi_3O_8$ feldspars. Dashed lines show the behavior of the cell parameters of the (metastable) paraelastic monoclinic structure in the stability field of the triclinic structure.

C2/m–C$\bar{1}$ PHASE TRANSITION IN DISORDERED $(Na,K)AlSi_3O_8$

Lattice-energy calculations

Starting from the triclinic disordered structure of $NaAlSi_3O_8$ given by Prewitt et al. (1976), with a single average position for the M site, we conducted static lattice calculations across the solid solution. The tetrahedral site occupancies were set at a completely disordered configuration by using a mixed potential corresponding to 0.25 Al and 0.75 Si on each T site, employing the method described by Equation 4. The structure minimized to a triclinic cell for Na-rich compositions, but the triclinic structure became increasingly unstable (as determined by lattice energies) with respect to the monoclinic paraphase with increasing K content. The paraphase could be simulated as a metastable solution in the triclinic stability field by minimizing from monoclinic starting coordinates (using those for sanidine given by Phillips and Ribbe 1973). Hence, properties such as spontaneous strain can be accurately calculated without any need to extrapolate the monoclinic cell parameters from those calculated for K-rich compositions.

The unit-cell parameters obtained from the lattice-energy calculations are given in Figure 1, and Figure 2a is a plot of the spontaneous strain components ϵ_4 and ϵ_6 as functions of K^+ content. The results are broadly consistent with the experimental observations, with the phase transition at $T = 0$ K occurring at a composition of about 22.5 mol% $KAlSi_3O_8$. Although this K content is significantly lower than that of about 34.4 mol% $KAlSi_3O_8$ observed experimentally (Kroll et al. 1986), it is noteworthy that the simple transferable potential employed here replicates the phase transition at all in such a complex aluminosilicate material because it represents a very small energetic perturbation of the total computed lattice energy. Although the composition predicted for the phase transition by computation is somewhat more albitic than that observed in real crystals, it must be remembered that the energy surface becomes very shallow close to the transition and the discrepancy in composition is likely to result from a small error in the formulation of the poten-

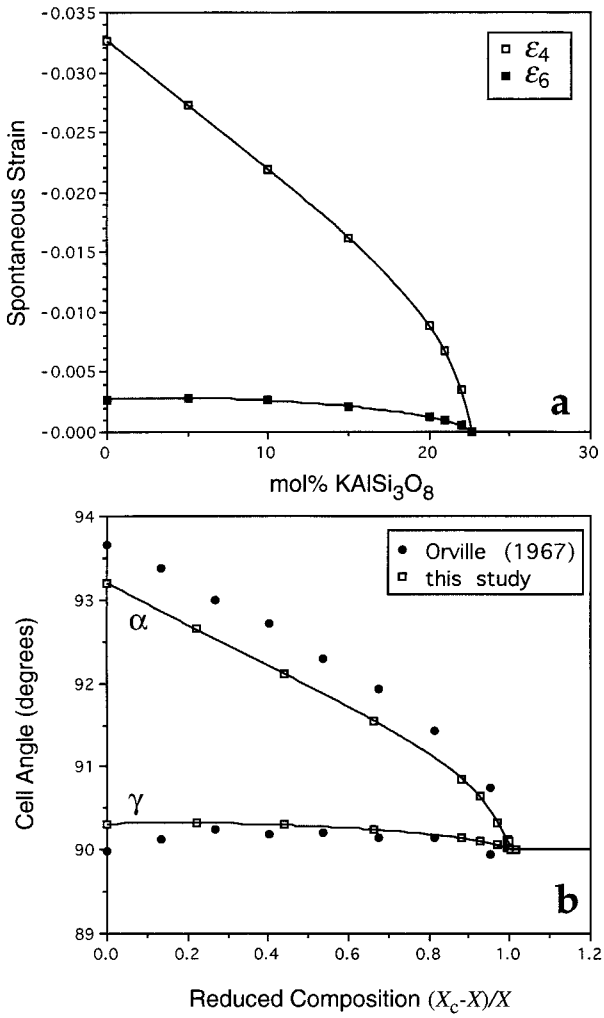

FIGURE 2. (**a**) Composition dependence of the calculated strains ϵ_4 and ϵ_6 in disordered $(Na,K)AlSi_3O_8$ feldspar. (**b**) Comparison of the measured (Orville 1967) and calculated triclinic α and γ cell angles in disordered triclinic alkali feldspars shown as a function of reduced composition (where X_c is the phase-transition composition).

tial for one of the end-member M cations. Nonetheless, the general trends and even the detailed structural behavior below the transition are replicated remarkably well. The spontaneous strains, for example, are seen to be consistent with the experimentally observed behavior, when the calculated and experimentally observed results appear together on a scale of reduced composition (Fig. 2b). This implies that the computed elastic properties are similarly reliable. We observe that ϵ_6 and ϵ_4 are linearly related close to the transition, becoming increasingly nonlinear (due to a reduction in ϵ_6) near the albite end-member (Fig. 3), as is also observed experimentally (with the γ angle becoming smaller near the albite end-member, Fig. 2b).

The computed elastic constants C_{44}, C_{66}, and C_{46} of the

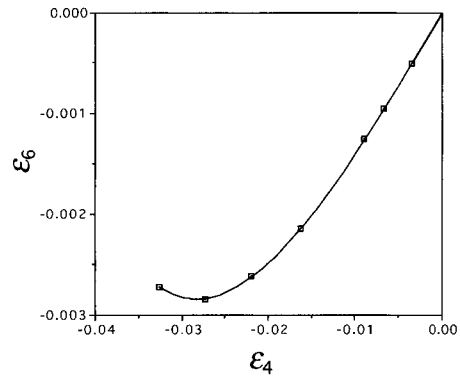

FIGURE 3. Relationship between the strains ϵ_4 and ϵ_6 in disordered $(Na,K)AlSi_3O_8$ feldspar.

alkali feldspars are shown in Figure 4, along with the critical combination $C_{44}C_{66} - C_{46}^2$. There is a weak dependence of the individual elastic constants on K^+ content, with C_{44} varying the most and C_{66} varying least, but because of the relative softness of C_{46} at all compositions the combination $C_{44}C_{66} - C_{46}^2$ becomes very sensitive to K^+ content. It can be seen that $C_{44}C_{66} - C_{46}^2$ falls to zero at the phase transition, a behavior that is consistent with a proper ferroelastic phase transition driven by an acoustic instability.

Lattice dynamics calculations

The calculated frequency of the lowest energy optic phonon with zero wave vector vs. K^+ content demonstrates that the elastic instability is not accompanied by any optic phonon softening, so that the transition is driven by an elastic softening alone (Fig. 5). In this way, we see that lattice dynamic and static lattice calculations can identify the important mechanisms associated with these types of phase transitions in complex solids.

I2/c–I$\bar{1}$ PHASE TRANSITION IN $(Ca,Sr)Al_2Si_2O_8$

Calculations on the Al-Si ordered solid solution

The monoclinic-to-triclinic transition in the $(Ca_xSr_{1-x})\cdot Al_2Si_2O_8$ feldspar solid solution is of interest because this system provides a means of investigating coupling between Al-Si order-disorder and ferroelastic behavior in the 2:2 Al:Si anorthite structure. Although $I\bar{1}$ anorthite remains highly ordered up to its melting point, there is nonetheless a measurable decrease in Al-Si order with temperature as the structure approaches a transition to a disordered $C\bar{1}$ state (Carpenter et al. 1990). A further transition from $C\bar{1}$ to $C2/m$ is anticipated at even higher temperatures (Carpenter 1992). The coupling between the zone-center monoclinic-to-triclinic transition and the zone-boundary tetrahedral order-disorder process can be investigated experimentally across the $(Ca,Sr)Al_2Si_2O_8$ solid solution, where substitution of Sr for Ca induces a phase transition from $I\bar{1}$ to $I2/c$ near the $SrAl_2Si_2O_8$ end-member (McGuinn and Redfern 1994a, 1994b; Tribau-

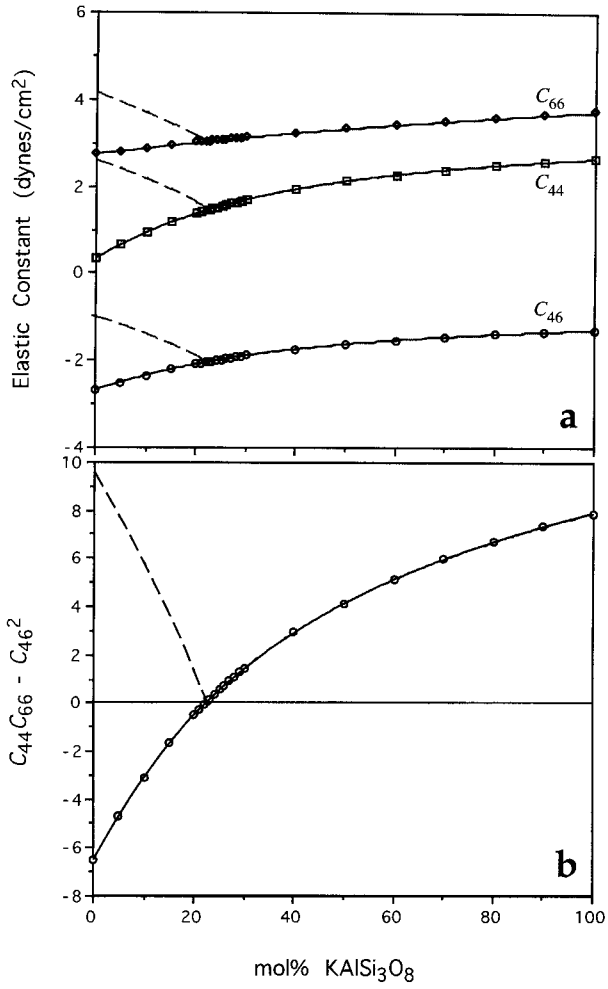

FIGURE 4. (**a**) Composition dependence of the elastic constants C_{44}, C_{66}, and C_{46} in disordered (Na,K)$AlSi_3O_8$ feldspar. Solid lines show the computed elastic constants of the *C*2/*m* structure, and dashed lines show the elastic constants of the relaxed $C\bar{1}$ structure. (**b**) Composition dependence of the critical combination of elastic constants, $C_{44}C_{66} - C_{46}^2$, in disordered (Na,K)$AlSi_3O_8$ feldspar, showing that this combination passes through zero at the *C*2/*m*–$C\bar{1}$ phase transition.

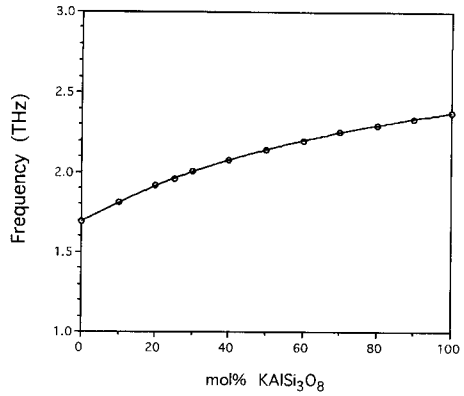

FIGURE 5. Composition dependence of the frequency of the lowest lying optic (**k** = 0) phonons in disordered (Na,K)$AlSi_3O_8$, demonstrating that the *C*2/*m*–$C\bar{1}$ phase transition is not accompanied by optic softening.

dino et al. 1993). We used mixed potentials for the M site to model this phase transition as a function of composition for (Ca,Sr)$Al_2Si_2O_8$ feldspars with perfect Al-Si order, and for the same solid solution with lower degrees of Al-Si order, and are able to identify the driving mechanisms and pertinent structural responses associated with the displacive phase transition.

We used the known structures of the *I*2/*c* $SrAl_2Si_2O_8$ end-member (Chiari et al. 1975) and $I\bar{1}$ anorthite (Kempster et al. 1962) for our starting coordinates and successively computed the properties of triclinic and monoclinic members of the intermediate solid solution in a manner analogous to that described above for the disordered alkali feldspars. In the $(Ca_xSr_{1-x})Al_2Si_2O_8$ solid solution, however, the results indicate that the triclinic phase is stable across the whole composition range at 0 K, which is in agreement with the anticipated form of the temperature-composition phase diagram described by Tribaudino (1994). The computational method adopted here enables fictive compositions beyond the end-members to be probed, however, by simply computing structures with negative Ca content (setting $x < 0$ in the formula unit and Equation 4). For example, a transition to *I*2/*c* would occur for completely ordered (Ca,Sr)$Al_2Si_2O_8$ feldspars near 102.5 mol% $SrAl_2Si_2O_8$, as is shown by Figure 6. The nature of the elastic instability is revealed by the behavior of the C_{44}, C_{66}, and C_{46} elastic constants. Lattice dynamic calculations across the solid solution demonstrate that the transition results from elastic instability alone, with no significant softening of optic modes (Fig. 7). Similar to the alkali feldspar solid solution, the results indicate that the transition is driven by the softening of the combination $C_{44}C_{66} - C_{46}^2$, which goes to zero at the transition. The discontinuities in the computed cell parameters (and derived spontaneous strains) and elastic constants indicate that the transition is first order in character, although not strongly so.

The computational results show that, because the transition is driven by only an acoustic instability, the strain ϵ_4 behaves as the primary order parameter for the ferroelastic transition. The other nonzero strain, ϵ_6, is coupled to ϵ_4 in a highly nonlinear manner (Fig. 8). In fact, the coupling between ϵ_6 and ϵ_4 in this solid solution is similar to that shown in the alkali feldspars (Fig. 3), the only difference being that the transition in the (Ca,Sr)$Al_2Si_2O_8$ feldspars is first-order: The linear (small strain) regime is not observed, and the values of ϵ_6 and ϵ_4 bypass the linear region upon transformation to the triclinic phase. It has long been known that ferroelastic transitions most strongly influence the α cell angle in feldspars (e.g., Salje et al. 1985). The γ cell angle has previously been recognized to vary nonuniformly with α in triclinic feldspars. It has also been demonstrated, however, that Al-Si order-disorder (described by an order parameter Q_{od}) most strongly

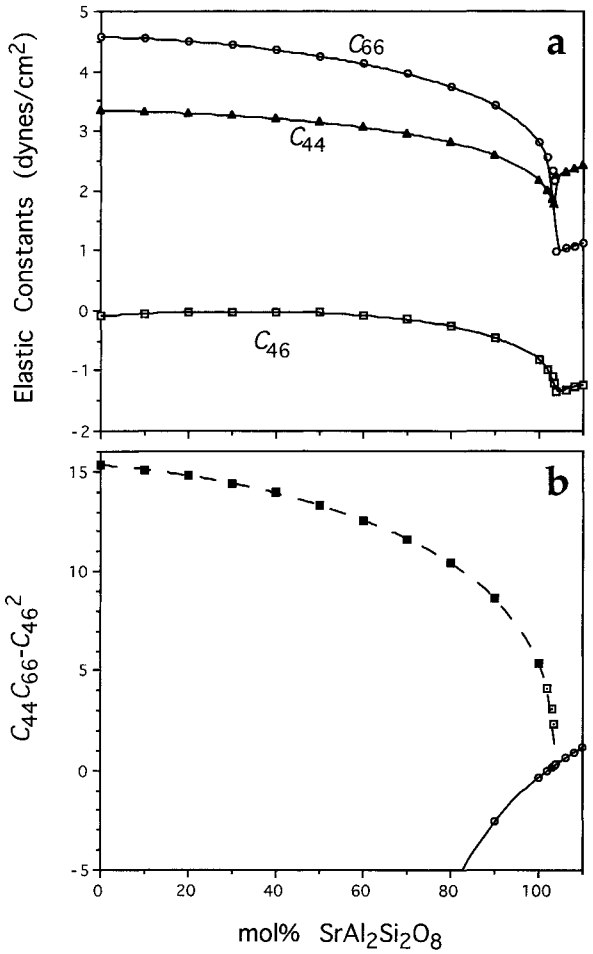

FIGURE 6. (a) Composition dependence of the elastic constants C_{44}, C_{66}, and C_{46} in ordered (Ca,Sr)$Al_2Si_2O_8$ feldspar. (b) Composition dependence of the critical combination of elastic constants, $C_{44}C_{66} - C_{46}^2$, in ordered (Ca,Sr)$Al_2Si_2O_8$ feldspar. Solid lines show the computed elastic constants of the *I*2/*c* structure, and dashed lines show the elastic constants of the relaxed $I\bar{1}$ structure.

affects γ. Hence, nonlinearity between α and γ at displacive transitions in feldspars has previously been attributed to coupled changes in Al-Si order, which induce variations in γ. Our results show, however, that such nonlinearity between the two triclinic cell angles occurs inherently in the absence of changes in Al-Si order, and possible variations in Q_{od} need not be invoked to explain the apparently strange composition dependence of γ. We notice that γ increases from zero at the transition from *I*2/*c* to $I\bar{1}$ and then decreases on further increase of Ca content. Because we know that Q_{od} couples strongly and positively to γ, we might expect these marked changes in γ to favor an increase in Q_{od} across the phase transition with a subsequent gradual reduction in Q_{od} with increasing Ca content. Such a change in Al-Si order associated with increasing Ca content across the *I*2/*c*-to-$I\bar{1}$ phase

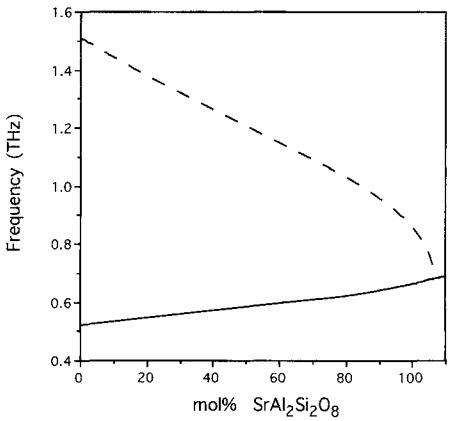

FIGURE 7. Composition dependence of the frequency of the lowest lying optic ($\mathbf{k} = 0$) phonons in ordered (Ca,Sr)$Al_2Si_2O_8$. The solid line shows the composition dependence of the lowest lying optic phonon in the monoclinic phase, and the dashed line shows the same for the relaxed triclinic structure. The results demonstrate that the *I*2/*c*–$I\bar{1}$ phase transition is not driven by optic softening but reveal that the coupling occurs between the optic hard-mode frequency and the strain behavior.

transition has indeed been observed experimentally in a recent NMR study (Phillips et al. 1997).

Influence of Al-Si order on the *I*2/c-to-$I\bar{1}$ transition

We also examined the influence of Al-Si order on the *I*2/*c*-to-$I\bar{1}$ transition by conducting static lattice calculations of the $(Ca_xSr_{1-x})Al_2Si_2O_8$ solid solution with varying degrees of Q_{od} ($2y - 1$, where y is the amount of Al on a T site that contains 100% Al in the ordered phase). The results are summarized in Figures 9 and 10, where they are presented together with the experimentally observed room-temperature cell parameters given by McGuinn and Redfern (1994a). The composition at which the *I*2/*c*-to-$I\bar{1}$ phase transition occurs, X_c, moves toward that of anorthite with decreasing Q_{od}, and the transition becomes

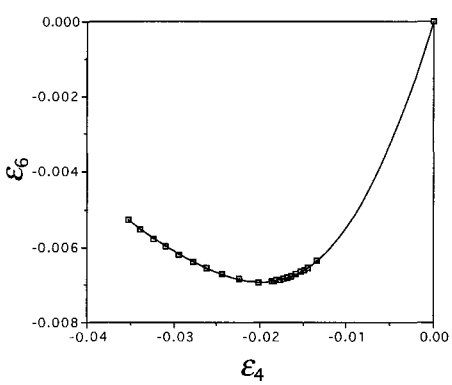

FIGURE 8. Relationship between the strains ϵ_4 and ϵ_6 in ordered (Ca,Sr)$Al_2Si_2O_8$ feldspar. The relationship is similar to that shown for alkali feldspars (Fig. 3), but because the *I*2/*c*–$I\bar{1}$ phase transition is computed as first order at 0 K, the observed strains fall in the region of strong nonlinearity.

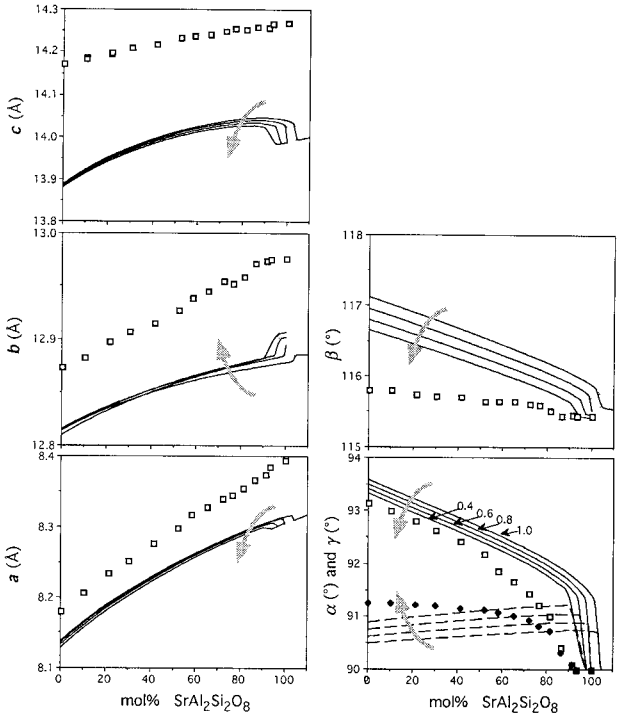

FIGURE 9. Composition dependence of the 0 K computed (lines) and 293 K observed (points; McGuinn and Redfern 1994a) cell parameters of $(Ca,Sr)Al_2Si_2O_8$ feldspars. Calculations for feldspars with tetrahedral Al-Si order (Q_{od}) ranging from 1.0 to 0.4 are shown, and large arrows indicate the general trend of each cell parameter on increasing disorder. In the plot of α and γ, α is shown by solid lines (computed) and open squares (observed), and γ is shown by dashed lines (computed) and solid diamonds (observed).

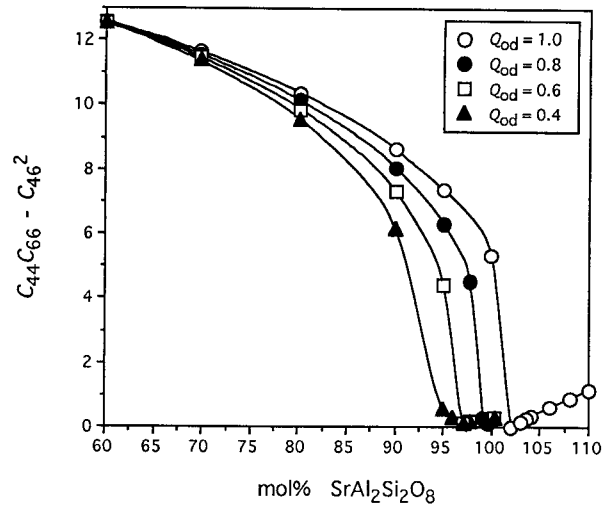

FIGURE 10. Composition and Q_{od} dependence of the critical combination of elastic constants, $C_{44}C_{66} - C_{46}^2$, in $(Ca,Sr)Al_2Si_2O_8$ feldspars. Decreasing order shifts the composition at which the $I2/c$–$I\bar{1}$ phase transition occurs toward $CaAl_2Si_2O_8$ and makes the transition less first order in character.

less first order in character (as shown by the slope at which the critical combination of elastic constants approaches zero as a function of composition). Tribaudino et al. (1993, 1995) observed that for disordered samples, which have T_c near room temperature, grains of both monoclinic and triclinic material coexist, suggesting that the transition becomes more first order on increasing Al-Si disorder. However, the possibility of chemical inhomogeneity within their samples was not fully addressed, and this may also be expected to induce a two-phase, apparently first-order regime near the transition point. In contrast, our model simulates a perfectly homogeneous, completely mean-field behavior, neglecting the effects of compositional or entropic fluctuations. In addition, Tribaudino et al. (1993) indicated that X_c shifts toward anorthite by 15 mol% or more for the disordered solid solution. Our 0 K calculations indicate that X_c moves only 5 mol% or less toward anorthite for the fully disordered solid solution. In this case, the effect of Al-Si disorder on the T-X phase diagram of $(Ca_xSr_{1-x})Al_2Si_2O_8$ feldspars is not only to shift the phase boundary of the $I2/c$-to-$I\bar{1}$ transition toward anorthite, but also to reduce the slope, dT/dX, of that phase boundary (Fig. 11).

DISCUSSION

Mechanism of the monoclinic-to-triclinic ferroelastic phase transition in feldspars

Our calculations indicate that the monoclinic-to-triclinic ferroelastic phase transition in feldspars is driven by an instability associated with the combination of elastic constants $C_{44}C_{66} - C_{46}^2$, rather than the softening of an optic phonon. The elastic instability does not result from softening of a single elastic constant, but strictly as the balance between the three elastic constants.

These results can be compared with the rigid-unit-mode (RUM) analysis of the stability of feldspar by Hammonds et al. (1996). This work showed that there is no low-energy optical distortion of the structure possible at $\mathbf{k} = 0$, but there is a general softening of several of the acoustic modes. Furthermore, the RUM model suggests that the elastic properties are determined by the forces associated with flexing of the T–O–T bonds and the interactions between alkali cations and the O^{2-} anions rather than the stiffness of the TO_4 tetrahedra. Thus, the present study confirms the prediction of the RUM model that the monoclinic-to-triclinic phase transition in feldspar is driven by an elastic softening.

Use of lattice-energy calculations of displacive phase transitions

The fact that we observed phase transitions at all in the solid solutions studied further validates the potential model that we employed. Much has been written on the model, particularly with reference to its ability to be transferred to different aluminosilicates and still retain its predictive power (Price et al. 1987; Catlow 1988; Dove 1989; Winkler et al. 1991; Patel et al. 1991). In the pres-

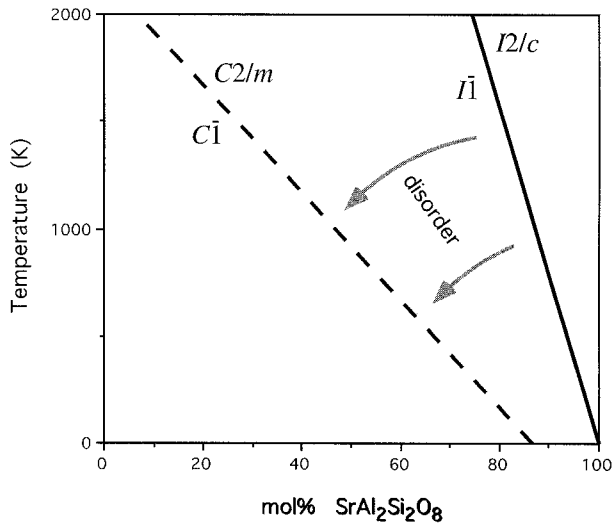

FIGURE 11. Schematic of the effect of tetrahedral disorder on the expected *T-X* phase diagram of $(Ca,Sr)Al_2Si_2O_8$ feldspars. Disorder shifts the phase boundary toward $CaAl_2Si_2O_8$ and reduces its *T-X* slope.

ent case it is essential that the potential energy has a shallow minimum that allows for easy distortion of the structure and has a shape that can change from a single minimum to a double minimum across the concentration range. This results from a very delicate balance between the interatomic interactions, which could in principle be significantly affected by small errors in the model. The success of the present model indicates that it captures the essential physical picture; the fact that the calculated critical compositions do not exactly match experiment is simply a reflection of the delicate nature of this balance. It is worth noting that the same model was also able to reproduce the main features associated with the displacive phase transition in leucite (Dove et al. 1993).

REFERENCES CITED

Burnham, C.W. (1990) The ionic model: Perceptions and realities in mineralogy. American Mineralogist, 75, 443–463.

Carpenter, M.A. (1992) Equilibrium thermodynamics of Al/Si ordering in anorthite. Physics and Chemistry of Minerals, 19, 1–24.

Carpenter, M.A., Angel, R.J., and Finger, L.W. (1990) Calibration of Al/Si order variations in anorthite. Contributions to Mineralogy and Petrology, 104, 471–480.

Catlow, C.R.A. (1988) Computer modeling of silicates. In E.K.H. Salje, Ed., Physical properties and thermodynamic behaviour of minerals, NATO ASI Series C, vol 225, p. 619–638. Reidel, Boston.

Chiari, G., Calleri, M., Bruno, E., and Ribbe, P.H. (1975) The structure of partially disordered synthetic strontium feldspar. American Mineralogist, 60, 111–119.

Cowley, R.A. (1976) Acoustic phonon instabilities and structural phase transitions. Physical Review, B13, 4877–4885.

Dove, M.T. (1989) On the computer modeling of diopside: Toward a transferable potential for silicate minerals. American Mineralogist, 74, 774–779.

Dove, M.T., Cool, T., Palmer, D.C., Putnis, A., Salje, E.K.H., and Winkler, B. (1993) On the role of Al-Si ordering in the cubic-tetragonal phase transition in leucite. American Mineralogist, 78, 486–492.

Hammonds, K.D., Dove, M.T., Giddy A.P., Heine V., and Winkler B. (1996) Rigid-unit phonon modes and structural phase transitions in framework silicates. American Mineralogist, 81, 1057–1079.

Kempster, C.J.E., Megaw, H.D., and Radoslovich, E.W. (1962) The structure of anorthite, $CaAl_2Si_2O_8$: I. Structure analysis. Acta Crystallographica, 15, 1005–1017.

Kroll, H., Schmiemann, I., and von Cölln, G. (1986) Feldspar solid solutions. American Mineralogist, 71, 1–16.

McGuinn, M.D., and Redfern, S.A.T. (1994a) Ferroelastic phase transition along the join $CaAl_2Si_2O_8$-$SrAl_2Si_2O_8$. American Mineralogist, 79, 24–30.

——(1994b) Ferroelastic phase transition in $SrAl_2Si_2O_8$ feldspar at elevated pressure. Mineralogical Magazine, 58, 21–26.

Orville, P.M. (1967) Unit-cell parameters of the microcline-low albite and the sanidine-high albite solid solution series. American Mineralogist, 52, 55–86.

Patel, A., Price, G.D., and Mendelssohn, M.J. (1991) A computer simulation approach to modeling the structure, thermodynamic and oxygen isotope equilibria of silicates. Physics and Chemistry of Minerals, 17, 690–699.

Phillips, B.L., McGuinn, M.D., and Redfern, S.A.T. (1997) Si/Al order and the $I\bar{1}$-*I2/c* structural phase transition in synthetic $CaAl_2Si_2O_8$-$SrAl_2Si_2O_8$ feldspars: A ^{29}Si MAS-NMR spectroscopic study. American Mineralogist, 82, 1–7.

Phillips, M.W., and Ribbe, P.H. (1973) The structures of monoclinic potassium-rich feldspars. American Mineralogist, 58, 263–270.

Post, J.E., and Burnham, C.W. (1987) Structure-energy calculations on low and high albite. American Mineralogist, 72, 507–514.

Prewitt, C.T., Sueno, S., and Papike, J.J. (1976) The crystal structures of high albite and monalbite at high temperatures. American Mineralogist, 61, 1213–1225.

Price, G.D., Parker, S.C., and Leslie, M. (1987) The lattice dynamics and thermodynamics of the Mg_2SiO_4 polymorphs. Physics and Chemistry of Minerals, 15, 181–190.

Purton, J., and Catlow, C.R.A. (1990) Computer simulation of feldspar structures. American Mineralogist, 75, 1268–1273.

Redfern, S.A.T., and Salje, E. (1987) Thermodynamics of plagioclase II: Temperature evolution of the spontaneous strain at the $I\bar{1}$-$P\bar{1}$ phase transition in anorthite. Physics and Chemistry of Minerals, 14, 189–195.

Salje, E., Kuscholke, B., and Wruck, B. (1985) Thermodynamics of sodium feldspar II: Experimental results and numerical calculations. Physics and Chemistry of Minerals, 12, 99–107.

Tribaudino, M. (1994) Al-Si ordering in Sr-rich feldspars of the join $CaAl_2Si_2O_8$-$SrAl_2Si_2O_8$: Spontaneous strain and TEM data. In A. Putnis, Ed., Kinetics of cation ordering, European Science Foundation Workshop, p. 51–58. Cambridge, U.K.

Tribaudino, M., Benna, P., and Bruno, E. (1993) $I\bar{1}$-*I2/c* phase transition in the alkaline earth feldspars along the $CaAl_2Si_2O_8$-$SrAl_2Si_2O_8$ join: Thermodynamic behaviour. Physics and Chemistry of Minerals, 20, 221–227.

——(1995) $I\bar{1}$-*I2/c* phase transition in the alkaline-earth feldspars: Evidence from TEM observations of Sr-rich feldspars along the $CaAl_2Si_2O_8$-$SrAl_2Si_2O_8$ join. American Mineralogist, 80, 907–915.

Winkler, B., Dove, M.T., and Leslie, M. (1991) Static lattice energy minimization and lattice dynamics calculations on aluminosilicate minerals. American Mineralogist, 76, 313–331.

MANUSCRIPT RECEIVED JANUARY 28, 1996
MANUSCRIPT ACCEPTED OCTOBER 4, 1996